

# Improving the sensitivity of Higgs boson searches in the golden channel

James S. Gainer<sup>a,b</sup>, Kunal Kumar<sup>b</sup>, Ian Low<sup>a,b</sup>, and Roberto Vega-Morales<sup>b</sup>

<sup>a</sup> *High Energy Physics Division, Argonne National Laboratory, Argonne, IL 60439*

<sup>b</sup> *Department of Physics and Astronomy, Northwestern University, Evanston, IL 60208*

## Abstract

Leptonic decays of the Higgs boson in the  $ZZ^{(*)}$  channel yield what is known as the golden channel due to its clean signature and good total invariant mass resolution. In addition, the full kinematic distribution of the decay products can be reconstructed, which, nonetheless, is not taken into account in traditional search strategy relying only on measurements of the total invariant mass. In this work we implement a type of multivariate analysis known as the matrix element method, which exploits differences in the full production and decay matrix elements between the Higgs boson and the dominant irreducible background from  $q\bar{q} \rightarrow ZZ^{(*)}$ . Analytic expressions of the differential distributions for both the signal and the background are also presented. We perform a study for the Large Hadron Collider at  $\sqrt{s} = 7$  TeV for Higgs masses between 175 and 350 GeV. We find that, with an integrated luminosity of  $2.5 \text{ fb}^{-1}$  or higher, improvements in the order of 10 – 20% could be obtained for both discovery significance and exclusion limits in the high mass region, where the differences in the angular correlations between signal and background are most pronounced.

## I. INTRODUCTION

The discovery of the Higgs boson [1] would be the triumphant culmination of the experimental quest to discover the particles of the Standard Model. The Tevatron has already set interesting limits on the Standard Model (SM) Higgs boson in the intermediate mass range [2]. At the Large Hadron Collider (LHC), with data corresponding to roughly  $1 \text{ fb}^{-1}$  of integrated luminosity, the ATLAS collaboration has announced exclusions at 95% confidence level of Higgs masses in the ranges  $155 - 190 \text{ GeV}$  and  $295 - 450 \text{ GeV}$  [3], while the CMS collaboration's limits are in the ranges  $149 - 206 \text{ GeV}$  and  $300 - 440 \text{ GeV}$  [4]. High mass limits from both collaborations are driven by measurements in the  $ZZ^{(*)}$  channel, which is considered the main discovery channel of the Higgs boson for masses above  $200 \text{ GeV}$ .

Among the different decay products of the Higgs into  $ZZ^{(*)}$  bosons, the one with both  $Z$  bosons decaying into  $e^+e^-$  or  $\mu^+\mu^-$  is often referred to as “the golden channel” because of the good invariant mass resolution and well-controlled background. The traditional search strategy using the golden channel thus focuses on measuring the invariant mass spectrum of the four leptons. However, given that four-momenta of all decay products can be reconstructed with sufficient resolution, it is possible to measure more than just the total invariant mass of the four leptons. In fact, there are a total of five angles (and two additional invariant masses, those of the off-shell  $Z$  bosons) that can be measured. Obviously it would be advantageous to incorporate all available kinematic information when searching for the Higgs boson.

Additional kinematic variables can be included in an experimental measurement by multivariate analyses [5], which already have a wide range of applications in many measurements done at the Tevatron and the  $B$  factories. Several multivariate methods have been employed, such as neural nets; boosted decision trees; and the Matrix Element Method (MEM) [6], the best-known use of which has been in studying the top quark at the Tevatron [7]. Even in some of the LHC Higgs analyses, most notably leptonic decays of Higgs to  $W^+W^-$  where there are two missing neutrinos, multivariate analyses, in particular boosted decision trees, have been used to incorporate additional kinematic observables such as the opening angle between the two charged leptons in the final states [8]. On the other hand, it is somewhat surprising that in the golden channel, where there is no missing particle in the final state and all angles can be reconstructed, no experimental analysis that we are aware of has considered

supplementing total invariant mass with angular correlations to search for the Higgs boson. (For recent analyses, see [3, 9].)

Angular correlations of Higgs decays in the golden channel have been studied previously, to determine the spin and CP properties of the putative Higgs resonance [10, 11]. A particularly useful observable, the azimuthal angle between the decay planes of the two  $Z$  bosons, was pointed out recently in Refs. [12, 13]. Subsequently, two comprehensive studies appeared in Refs. [14, 15]. These works included the computation of the angular correlations of the final state leptons resulting from the production of a resonance (with arbitrary spin less than or equal to two) which in turn decays, via general couplings, to a pair of  $Z$  bosons, which subsequently decay leptonically. Both analyses also implemented the MEM in this  $ZZ^{(*)} \rightarrow 4\ell$  channel, to distinguish between various hypotheses for the spin and CP properties of the putative Higgs signal at the LHC with  $\sqrt{s} = 14$  and 10 TeV, respectively. Moreover, Ref. [15] briefly discussed using the MEM to enhance the Higgs discovery reach in the golden channel at 10 TeV for two specific values of the Higgs mass (200 and 350 GeV).

In the present work, instead of comparing angular correlations for different spin and CP assumptions for a singly produced resonance, we aim at distinguishing the SM Higgs boson signal from the dominant irreducible background  $q\bar{q} \rightarrow ZZ^{(*)} \rightarrow 4\ell$  using the MEM at the LHC with  $\sqrt{s} = 7$  TeV. The scattering amplitude for  $q\bar{q} \rightarrow ZZ^{(*)} \rightarrow 4\ell$ , when both  $Z$  bosons are on-shell, has been computed long ago in Refs. [16, 17]. We extend the calculation of Ref. [17] to off-shell  $Z$  bosons and present analytic expressions for the fully differential cross section. Then we perform a Monte Carlo study, implementing the MEM to determine the improvement in sensitivity for Higgs boson searches in the golden channel over a significant range of Higgs masses (between 175 and 350 GeV). We perform these analyses for several integrated luminosities, between 1 and 7.5 fb<sup>-1</sup>. For simplicity we consider only the 0-jet bin and assume that events have no intrinsic  $p_T$ , though we expect the qualitative features of our results to be more generally applicable.

This work is organized as follows: in Sect. II we introduce and define kinematic variables to be used in the fully differential cross sections. In particular, Lorentz-invariant expressions for all production and decay angles are presented, so that the kinematic distributions can be reconstructed using measurements done in the laboratory frame. In Sect. III we compute the amplitude and cross section for  $q\bar{q} \rightarrow ZZ^{(*)} \rightarrow 4\ell$  using the technique of helicity amplitudes introduced in Ref. [18], allowing both  $Z$  bosons to be off-shell. In Sect. IV the

MEM is briefly reviewed, as well as the relevant statistical procedures we employed. The Monte Carlo study, including event generation, detector smearing effects, and construction of pseudo-experiments is discussed in Sect. V. Then we present our results for both expected significance and exclusion limits in Sect. VI. Finally, we close with conclusions in Sect. VII.

## II. KINEMATICS

As noted above, in this study we consider events in which two  $Z$  bosons are produced, either from the decay of a SM Higgs Boson produced in the gluon fusion channel or from  $t(u)$ -channel  $q\bar{q}$  production. Each  $Z$  boson, which could be either on or off the mass shell, decays to a lepton ( $\ell$ ) and an anti-lepton ( $\bar{\ell}$ ). We do not consider events with additional particles in the final state; thus the transverse momentum of the  $4\ell$  system is assumed to be negligible. In other words, we only consider exclusive  $ZZ^{(*)} \rightarrow 4\ell$  processes.

In these events, the final state can be completely reconstructed. In general the kinematics can be specified in terms of two production angles of the  $ZZ^{(*)}$  system, one of which is irrelevant; four decay angles describing  $ZZ^{(*)} \rightarrow 4\ell$ ; and the invariant masses of the  $Z$ 's. In hadron colliders it is also necessary to know the momentum fractions of the initial massless partons,  $x_1$ , and  $x_2$ , in order to compute the differential cross sections. We now describe our convention for the angles which specify the event and how to obtain them for a particular event. In particular, we provide Lorentz-invariant definitions of all angles, allowing for their determination from four-momenta reconstructed in the laboratory (Lab) frame.

### A. Definition of angles

Let  $p_1$  and  $p_2$  be the momenta of the lepton pair coming from  $Z_1$ , and  $p_3$  and  $p_4$  be the momenta of the lepton pair from  $Z_2$ , while  $k_{1,2}$  are the momenta of  $Z_{1,2}$ . Our notation is such that  $p_1 = \ell_1$ ,  $p_2 = \bar{\ell}_1$ ,  $p_3 = \ell_2$ ,  $p_4 = \bar{\ell}_2$ , i.e.  $p_1$  is the momentum of the lepton from  $Z_1$  decay,  $p_2$  the momentum of the antilepton from  $Z_1$  decay, etc. We denote the momenta of the incoming partons by  $k_q$  and  $k_{\bar{q}}$ . The total momentum of the  $ZZ^{(*)}$  system is  $P = k_q + k_{\bar{q}} = k_1 + k_2 = p_1 + p_2 + p_3 + p_4$ , which satisfies  $P^2 = \hat{s} \equiv M^2$ . For Higgs production in the gluon fusion channel, the incoming partons are self-conjugate,  $k_q = k_{\text{gluon},1}$ ,  $k_{\bar{q}} = k_{\text{gluon},2}$ , and the total momentum  $P$  is the Higgs momentum.

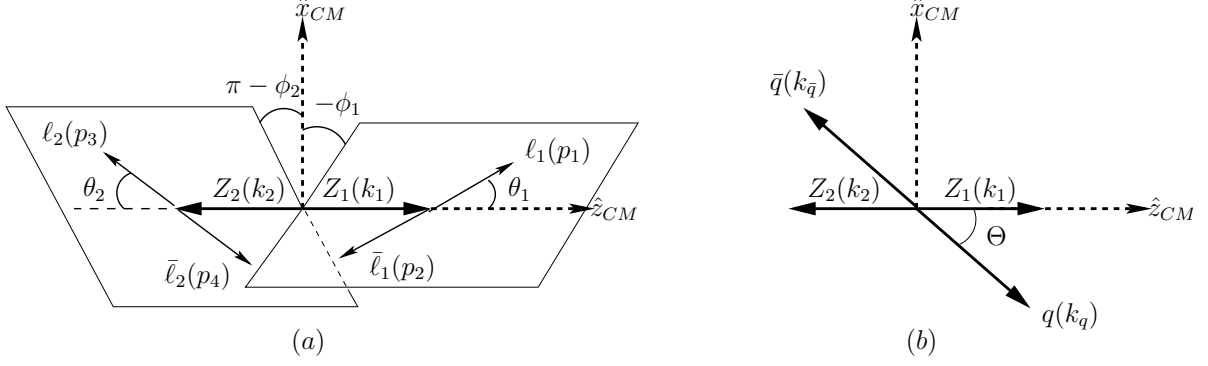


FIG. 1: (a) Two decay planes of  $Z_i \rightarrow \ell_i \bar{\ell}_i$ ,  $i = 1, 2$ . The polar angles  $\theta_i$  shown are defined in the rest frames of  $Z_i$  with respect to  $\hat{k}_i$ , while the azimuthal angles shown are in fact  $2\pi - \phi_1 = -\phi_1$  and  $\pi - \phi_2$ . (b) The coordinate system in the CM frame and the definition of the production angle  $\Theta$ .

As indicated in Fig. 1, we choose the coordinate system in the center-of-mass (CM) frame of the two  $Z$ 's system as:

$$\hat{z}_{CM} = \hat{k}_1, \quad \hat{y}_{CM} = \frac{\hat{k}_q \times \hat{k}_1}{|\hat{k}_q \times \hat{k}_1|}, \quad \hat{x}_{CM} = \hat{y}_{CM} \times \hat{z}_{CM} = \frac{-\hat{k}_q + \hat{k}_1(\hat{k}_q \cdot \hat{k}_1)}{|\hat{k}_q \times \hat{k}_1|}. \quad (1)$$

Furthermore, we define  $\mathcal{Z}_1$  as the rest frame of the  $Z_1$  boson by boosting the CM frame along  $\hat{k}_1$ , while  $\mathcal{Z}_2$  is obtained by first rotating CM frame with respect to  $\hat{y}_{CM}$  by  $\pi$  and then boosting along  $\hat{k}_2$ . The production angle  $\Theta$  and decay angles  $\{\theta_1, \theta_2, \phi_1, \phi_2\}$  are defined as follows:

- $\Theta$ : polar angle of the momentum of the incoming quark in the CM frame.
- $\theta_{1,2}$ : polar angle of the momentum of  $\ell_{1,2}$  in the  $\mathcal{Z}_{1,2}$  frame.
- $\phi_{1,2}$ : azimuthal angle of  $\ell_{1,2}$  in the  $\mathcal{Z}_{1,2}$  frame.

The azimuthal production angle is irrelevant and chosen to be zero. In these definitions, three-momenta of  $\ell_{1,2}$  in the  $\mathcal{Z}_{1,2}$  frame can be written as

$$\vec{p}_{\ell_i} \text{ in the } \mathcal{Z}_i \text{ frame} = |\vec{p}_{\ell_i}| (\sin \theta_i \cos \phi_i, \sin \theta_i \sin \phi_i, \cos \theta_i), \quad i = 1, 2, \quad (2)$$

while the three-momentum of the incoming parton in the CM frame is

$$\vec{k}_q \text{ in the CM frame} = |\vec{k}_q| (-\sin \Theta, 0, \cos \Theta). \quad (3)$$

In hadron colliders the CM frame of the two  $Z$ 's system is different from the Lab frame and the event as a whole will be boosted along the beam axis with respect to the Lab frame,  $P = (P^0, 0, 0, P^z)$ . Also, we have chosen to define the coordinate system in the CM frame such that the  $\hat{z}$  axis is defined by the  $Z_1$  three-momentum, rather than by the three-momentum of the incident partons, as is natural in the Lab frame.

The total energy and momentum of the event  $P$  in the Lab frame can be used to determine the momentum fractions of the incident partons. Following Ref. [19], we write  $k_q = x_1(E_{cm}, 0, 0, E_{cm})$  and  $k_{\bar{q}} = x_2(E_{cm}, 0, 0, -E_{cm})$ , where  $E_{cm} = \sqrt{s}/2$  is the CM energy of the colliding protons. From  $P = k_q + k_{\bar{q}}$  we see that  $\hat{s} = x_1 x_2 s$  and

$$k_q = \frac{1}{2}(P^0 + P^z, 0, 0, P^0 + P^z), \quad (4)$$

$$k_{\bar{q}} = \frac{1}{2}(P^0 - P^z, 0, 0, P^z - P^0), \quad (5)$$

which are valid in the Lab frame.

## B. Lorentz-invariant construction of angles

In the CM frame,  $\vec{k}_1$  and  $\vec{k}_2$  are back to back and of equal magnitude, as are  $\vec{k}_q$  and  $\vec{k}_{\bar{q}}$ . Using  $P = M(1, 0, 0, 0)$  we can work out the energy and three-momentum of the incoming partons,

$$E_q = E_{\bar{q}} = |\vec{k}_q| = |\vec{k}_{\bar{q}}| = \frac{\sqrt{\hat{s}}}{2}, \quad (6)$$

as well as that of the two  $Z$ 's,

$$E_i = \frac{P \cdot k_i}{M}, \quad |\vec{k}_i| = \sqrt{\left(\frac{P \cdot k_1}{M}\right)^2 - m_{12}^2} \equiv \lambda_Z, \quad i = 1, 2, \quad (7)$$

where we define  $m_{ij}^2 = (p_i + p_j)^2 = 2p_i \cdot p_j$ . Alternatively,  $\lambda_Z = \sqrt{(P \cdot k_2/M)^2 - m_{34}^2}$ .

Since  $\cos \Theta = \hat{k}_q \cdot \hat{k}_1$ , by computing  $k_q \cdot k_1$  it is simple to derive

$$\cos \Theta = \frac{-k_q \cdot k_1 + E_q E_1}{|\vec{k}_q| |\vec{k}_1|} = \frac{(k_{\bar{q}} - k_q) \cdot k_1}{M \lambda_Z}. \quad (8)$$

By definition  $\cos \Theta$  changes sign under  $\hat{k}_q \leftrightarrow \hat{k}_{\bar{q}}$ , which is manifest in Eq. (8). Thus when the direction of the incoming quark cannot be distinguished from the anti-quark, as is the case for hadron colliders, or when the incoming partons are self-conjugate as in the Higgs

production channel we consider, one can only determine  $\cos \Theta$  up to a minus sign. Because  $\Theta$  is only defined between 0 and  $\pi$ , it is not necessary to compute  $\sin \Theta$ .

Next we consider  $\theta_i$ , which was worked out in the appendix of Ref. [13]. Since  $k_1 = p_1 + p_2$ , in the CM frame we can write  $k_1 = (E_1 + E_2, 0, 0, |\vec{p}_1 + \vec{p}_2|)$  and solve for the boost that takes  $k_1$  from the CM frame to the rest frame of  $Z_1$  where it is  $(m_{12}, 0, 0, 0)$ :

$$\begin{pmatrix} m_{12} \\ 0 \end{pmatrix} = \begin{pmatrix} \gamma & -\gamma\beta \\ -\gamma\beta & \gamma \end{pmatrix} \begin{pmatrix} E_1 + E_2 \\ |\vec{p}_1 + \vec{p}_2| \end{pmatrix}, \quad (9)$$

from which we get

$$\beta = \frac{|\vec{p}_1 + \vec{p}_2|}{E_1 + E_2}, \quad \gamma = \frac{E_1 + E_2}{m_{12}}. \quad (10)$$

The inverse boost would then take  $p_1 = (m_{12}/2)(1, \sin \theta_1 \cos \phi_1, \sin \theta_1 \sin \phi_1, \cos \theta_1)$  in the  $Z_1$  rest frame to  $p_1 = (E_1, \vec{p}_1)$  in the CM frame, implying the following relation:

$$E_1 = \gamma \frac{m_{12}}{2} (1 + \beta \cos \theta_1), \quad (11)$$

from which we obtain

$$\cos \theta_1 = \frac{E_1 - E_2}{|\vec{p}_1 + \vec{p}_2|} = \frac{E_1 - E_2}{|\vec{k}_1|}. \quad (12)$$

Using Eq. (7) we arrive at

$$\cos \theta_1 = \frac{1}{M\lambda_Z} P \cdot (p_1 - p_2). \quad (13)$$

For  $\cos \theta_2$ , simply replace  $p_1$  and  $p_2$  by  $p_3$  and  $p_4$ , respectively, and we obtain

$$\cos \theta_2 = \frac{1}{M\lambda_Z} P \cdot (p_3 - p_4). \quad (14)$$

To compute  $\phi_i$ , we first construct the unit normal vectors of the two decay planes,

$$\hat{N}_1 = \frac{\vec{p}_1 \times \vec{p}_2}{|\vec{p}_1 \times \vec{p}_2|}, \quad \hat{N}_2 = \frac{\vec{p}_3 \times \vec{p}_4}{|\vec{p}_3 \times \vec{p}_4|}, \quad (15)$$

so that

$$\hat{N}_1 \cdot \hat{x}_{CM} = \sin \phi_1, \quad \hat{N}_1 \cdot \hat{y}_{CM} = -\cos \phi_1, \quad (16)$$

$$\hat{N}_2 \cdot \hat{x}_{CM} = -\sin \phi_2, \quad \hat{N}_2 \cdot \hat{y}_{CM} = -\cos \phi_2. \quad (17)$$

The numerator of the normal vector can be written as

$$(\vec{p}_i \times \vec{p}_j)^a = \frac{1}{M} \epsilon^{\mu\nu a \rho} p_{i\mu} p_{j\nu} P_\rho \equiv \frac{1}{M} \epsilon^{p_i p_j a P}, \quad (18)$$

where  $\epsilon_{0123} = -\epsilon^{0123} = 1$ . On the other hand, the Lorentz-invariant form of the numerator can be obtained using the relations

$$|\vec{p}_i| = \frac{1}{M} p_i \cdot P, \quad \cos \bar{\theta}_{ij} = 1 - \frac{m_{ij}^2}{2|\vec{p}_i||\vec{p}_j|}, \quad (19)$$

where  $\bar{\theta}_{ij}$  is the opening angle between  $\vec{p}_i$  and  $\vec{p}_j$  in the CM frame, so that in the end we have

$$|\vec{p}_i \times \vec{p}_j| = |\vec{p}_i||\vec{p}_j| \sin \bar{\theta}_{ij} = m_{ij} \left( \frac{p_i \cdot P}{M} \frac{p_j \cdot P}{M} - \frac{m_{ij}^2}{4} \right)^{\frac{1}{2}} \equiv \kappa_{ij}. \quad (20)$$

One then calculates

$$\sin \phi_1 = -\frac{\vec{p}_1 \times \vec{p}_2}{|\vec{p}_1 \times \vec{p}_2|} \cdot \frac{\hat{k}_q}{\sin \Theta} = \frac{2}{M^2 \kappa_{12} \sin \Theta} \epsilon^{p_1 p_2 k_q P}, \quad (21)$$

$$\cos \phi_1 = -\frac{\vec{p}_1 \times \vec{p}_2}{|\vec{p}_1 \times \vec{p}_2|} \cdot \frac{\hat{k}_q \times \hat{k}_1}{|\hat{k}_q \times \hat{k}_1|} = -\frac{2}{M^3 \kappa_{12} \lambda_Z \sin \Theta} \begin{vmatrix} p_1 \cdot k_q & p_1 \cdot k_1 & p_1 \cdot P \\ p_2 \cdot k_q & p_2 \cdot k_1 & p_2 \cdot P \\ P \cdot k_q & P \cdot k_1 & M^2 \end{vmatrix}, \quad (22)$$

and similarly

$$\sin \phi_2 = -\frac{2}{M^2 \kappa_{34} \sin \Theta} \epsilon^{p_3 p_4 k_q P}, \quad (23)$$

$$\cos \phi_2 = -\frac{2}{M^3 \kappa_{34} \lambda_Z \sin \Theta} \begin{vmatrix} p_3 \cdot k_q & p_3 \cdot k_1 & p_3 \cdot P \\ p_4 \cdot k_q & p_4 \cdot k_1 & p_4 \cdot P \\ P \cdot k_q & P \cdot k_1 & M^2 \end{vmatrix}. \quad (24)$$

It is also worth noting that when  $\hat{k}_q \rightarrow -\hat{k}_q$ ,  $\phi_i \rightarrow \pi + \phi_i$ . So in hadron colliders or gluon fusion production we cannot distinguish between an event described by angles  $(\Theta, \theta_1, \theta_2, \phi_1, \phi_2)$  and an event described by angles  $(\pi - \Theta, \theta_1, \theta_2, \phi_1 + \pi, \phi_2 + \pi)$ .

### III. DIFFERENTIAL CROSS SECTIONS

Angular distributions in  $ZZ^{(*)} \rightarrow 4\ell$  provide a wealth of information on the production mechanism of the two  $Z$  bosons [11–15, 20]. Similar angular correlations in the vector boson fusion channel of Higgs production have also been discussed in Ref. [21]. As noted above, in this work we focus on the search of the Higgs boson in the golden channel,  $h \rightarrow ZZ^{(*)} \rightarrow 4\ell$ , and study the possibility of differentiating the Higgs signal from the dominant irreducible background  $q\bar{q} \rightarrow ZZ^{(*)} \rightarrow 4\ell$  using spin correlations. In particular, we will compute the amplitudes in a helicity basis following Ref. [17].



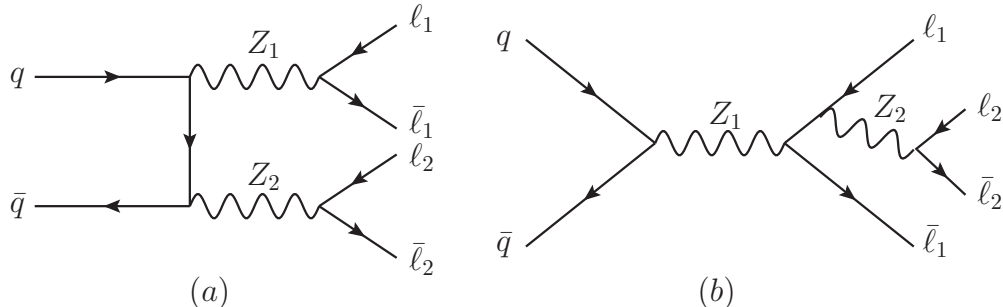


FIG. 2: *Feynman diagrams contributing to  $q\bar{q} \rightarrow 4\ell$ . We only consider (a), since final states from (b) have a total invariant mass at the  $Z$  mass.*

We will present the expressions for the fully differential cross section for both the signal and the background. Results for the Higgs production and decay have appeared in many previous works (see, for example, Refs. [11, 13–15, 22]) and are not new. They are given here for completeness. Earlier works on  $q\bar{q} \rightarrow ZZ^{(*)} \rightarrow 4\ell$  include [16, 17].

Feynman diagrams contributing to  $q\bar{q} \rightarrow 4\ell$  are shown in Fig. 2. We consider only the diagram in (a) and the corresponding  $u$ -channel diagram, as we are interested in final states with a total invariant mass much larger than the  $Z$  mass. We will compute the amplitude of the diagram in Fig. 2 (a) and its  $u$ -channel partner in a helicity basis, following Ref. [17]. The amplitude for the process under consideration factorizes into one production and two decay amplitudes:

$$q(k_q, \sigma) + \bar{q}(k_{\bar{q}}, \bar{\sigma}) \longrightarrow Z_1(k_1, \lambda_1) + Z_2(k_2, \lambda_2) , \quad (25)$$

$$Z_1(k_1, \lambda_1) \longrightarrow \ell_1(p_1, \sigma_1) + \bar{\ell}_1(p_2, \sigma_2) , \quad (26)$$

$$Z_2(k_2, \lambda_2) \longrightarrow \ell_2(p_3, \sigma_3) + \bar{\ell}_2(p_4, \sigma_4) , \quad (27)$$

where the momentum and helicity of each particle are indicated. A similar factorization obtains in the case of the  $gg \rightarrow h \rightarrow ZZ^{(*)} \rightarrow 4\ell$  signal. As the production and decay amplitudes factorize, we will consider them separately.

Before going into details of the computation, we state here the conventions we choose for various kinematic vectors and fermion spinors. We use the explicit expressions for the

four-momenta and polarization vectors of the  $Z$  bosons in the CM frame:

$$k_1 = m_1 \gamma_1 (1, 0, 0, \beta_1) , \quad (28)$$

$$k_2 = m_2 \gamma_2 (1, 0, 0, -\beta_2) , \quad (29)$$

$$\epsilon_1^{(\pm)} = \frac{1}{\sqrt{2}} (0, \mp 1, i, 0) , \quad \epsilon_1^{(0)} = \gamma_1 (\beta_1, 0, 0, 1) , \quad (30)$$

$$\epsilon_2^{(\pm)} = \frac{1}{\sqrt{2}} (0, \pm 1, i, 0) , \quad \epsilon_2^{(0)} = \gamma_2 (\beta_2, 0, 0, -1) , \quad (31)$$

where  $k_i^2 = m_i^2$ ,  $i = 1, 2$  is the invariant mass of  $Z_i$ , which could be off the mass shell, and the boost factors are

$$\gamma_1 = \frac{1}{\sqrt{1 - \beta_1^2}} = \frac{\sqrt{\hat{s}}}{2m_1} (1 + x) , \quad \gamma_2 = \frac{1}{\sqrt{1 - \beta_2^2}} = \frac{\sqrt{\hat{s}}}{2m_1} (1 - x) , \quad x = \frac{m_1^2 - m_2^2}{\hat{s}} . \quad (32)$$

We will also use the explicit forms of  $u(p, \lambda)$  and  $v(p, \lambda)$  spinors:

$$u_R = \begin{pmatrix} 0 \\ 0 \\ \sqrt{2E} \\ 0 \end{pmatrix} , \quad u_L = \begin{pmatrix} 0 \\ \sqrt{2E} \\ 0 \\ 0 \end{pmatrix} , \quad v_R = \begin{pmatrix} \sqrt{2E} \\ 0 \\ 0 \\ 0 \end{pmatrix} , \quad v_L = \begin{pmatrix} 0 \\ 0 \\ 0 \\ -\sqrt{2E} \end{pmatrix} , \quad (33)$$

where  $E$  is the energy (or momentum) of the massless lepton. In these expressions,  $u(p, \lambda)$  have been defined for  $p$  in the  $\hat{\mathbf{z}}$  direction and  $v(p, \lambda)$  have been defined for  $p$  in the  $-\hat{\mathbf{z}}$  direction. Our conventions here are those in [17, 18]; these were chosen so that our  $q\bar{q} \rightarrow ZZ^{(*)}$  helicity amplitudes would reduce to those in Ref. [17] in the limit where the  $Z$  bosons are on shell.

### A. Production amplitudes for the signal

Because the Higgs is a scalar particle, the two  $Z$  bosons can only have the following three helicity combinations:  $(0, 0)$  and  $(\pm 1, \pm 1)$ . Since the gluon-gluon-Higgs coupling is given by

$$\frac{\alpha_s}{12\pi v} h G_{\mu\nu} G^{\mu\nu} , \quad (34)$$

where  $v = 246$  GeV is the Higgs vev, the production helicity amplitude  $\mathcal{M}_{h;\lambda_1\lambda_2}^{ZZ}$  for  $gg \rightarrow h \rightarrow ZZ^{(*)}$  can be written as

$$\mathcal{M}_{h;\pm 1\pm 1}^{ZZ} = \frac{\alpha_s m_Z^2 \hat{s}}{3\pi v^2 ((\hat{s} - m_h^2)^2 + m_h^2 \Gamma_h^2)^{1/2}} , \quad (35)$$

$$\mathcal{M}_{h;00}^{ZZ} = \gamma_1 \gamma_2 (1 + \beta_1 \beta_2) \frac{\alpha_s m_Z^2 \hat{s}}{3\pi v^2 ((\hat{s} - m_h^2)^2 + m_h^2 \Gamma_h^2)^{1/2}} . \quad (36)$$

This is the amplitude for a particular spin and color configuration for the initial gluons. In the interest of clarity, we do not write the gluon helicities in the above amplitude, however these amplitudes should be taken as the amplitude for the  $++$  or  $--$  initial state gluon helicities. For the other two helicity combinations, the amplitude vanishes. We will average the squared sum of these amplitudes over spin and color when finding the differential cross section. It is worth pointing out that, as one can easily see from Eq. (35), in the high energy limit when the Higgs is heavy, the boost factor  $\gamma \gg 1$  and the amplitude for two longitudinal  $Z$  bosons,  $(\lambda_1, \lambda_2) = (0, 0)$ , dominate over those for the transverse  $Z$ s.

## B. Production amplitudes for the background

The production helicity amplitude for  $q\bar{q} \rightarrow Z_1 Z_2$  in the CM frame reads [17]

$$\mathcal{M}_{\sigma\bar{\sigma};\lambda_1\lambda_2}^{ZZ} = 4\sqrt{2} \left( g_{\Delta\sigma}^{Zq\bar{q}} \right)^2 \epsilon \delta_{|\Delta\sigma|, \pm 1} \frac{\mathcal{A}_{\lambda_1\lambda_2}^{\Delta\sigma}(\Theta) d_{\Delta\sigma, \Delta\lambda}^{J_0}(\Theta)}{4\beta_1\beta_2 \sin^2 \Theta + (1 - \beta_1\beta_2)^2 - x^2(1 + \beta_1\beta_2)^2} . \quad (37)$$

In the above  $\Delta\sigma = \sigma - \bar{\sigma}$ ,  $\epsilon = \Delta\sigma(-1)^{\lambda_2}$ ,  $\Delta\lambda = \lambda_1 - \lambda_2$ , and  $J_0 = \max(|\Delta\sigma|, |\Delta\lambda|)$ . Note that in the limit of massless quarks, which we consider in this work, the amplitude in Eq. (37) vanishes for  $\Delta\sigma = 0$ . The left- and right-handed coupling of quarks to the  $Z$  boson are given by:

$$g_{\Delta\sigma}^{Zq\bar{q}} = \frac{|e|(T_3 - Q \sin^2 \theta_W)}{\sin \theta_W \cos \theta_W}, \quad (38)$$

where  $T_3 = 0$  for right-handed quarks. Furthermore,  $d_{\Delta\sigma, \Delta\lambda}^{J_0}(\Theta)$  is the  $d$  function in the convention of the Particle Data Group [23]. The coefficients  $\mathcal{A}_{\lambda_1\lambda_2}^{\Delta\sigma}$  are

$$\Delta\lambda = \pm 2 : \quad \mathcal{A}_{\pm\mp}^{\Delta\sigma} = -\sqrt{2}(1 + \beta_1\beta_2), \quad (39)$$

$$\begin{aligned} \Delta\lambda = \pm 1 : \quad \mathcal{A}_{\pm 0}^{\Delta\sigma} &= \frac{1}{\gamma_2(1+x)} \left[ (\Delta\sigma\Delta\lambda) \left( 1 + \frac{\beta_1^2 + \beta_2^2}{2} \right) - 2 \cos \Theta \right. \\ &\quad \left. - (\Delta\sigma\Delta\lambda)(\beta_2^2 - \beta_1^2)x - 2x \cos \Theta - (\Delta\sigma\Delta\lambda) \left( 1 - \frac{\beta_1^2 + \beta_2^2}{2} \right) x^2 \right] \end{aligned} \quad (40)$$

$$\begin{aligned} : \quad \mathcal{A}_{0\pm}^{\Delta\sigma} &= \frac{1}{\gamma_1(1-x)} \left[ (\Delta\sigma\Delta\lambda) \left( 1 + \frac{\beta_1^2 + \beta_2^2}{2} \right) - 2 \cos \Theta \right. \\ &\quad \left. - (\Delta\sigma\Delta\lambda)(\beta_2^2 - \beta_1^2)x + 2x \cos \Theta - (\Delta\sigma\Delta\lambda) \left( 1 - \frac{\beta_1^2 + \beta_2^2}{2} \right) x^2 \right] \end{aligned} \quad (41)$$

$$\Delta\lambda = 0 : \quad \mathcal{A}_{\pm\pm}^{\Delta\sigma} = -(1 - \beta_1\beta_2) \cos \Theta - \lambda_1 \Delta\sigma (1 + \beta_1\beta_2)x, \quad (42)$$

$$\Delta\lambda = 0 : \quad \mathcal{A}_{00}^{\Delta\sigma} = 2\gamma_1\gamma_2 \cos \Theta \left[ ((1-x)\beta_1 + (1+x)\beta_2) \sqrt{\frac{\beta_1\beta_2}{1-x^2}} - (1 + \beta_1^2\beta_2^2) \right]. \quad (43)$$

It can be checked that in the on-shell limit when  $x \rightarrow 0$ ,  $\beta_1, \beta_2 \rightarrow \beta$ , and  $\gamma_1, \gamma_2 \rightarrow \gamma$ , the above expressions reduce to those presented in Appendix D of Ref. [17]. Moreover, in the high energy limit when  $\gamma \gg 1$ , the  $\Delta\lambda = \pm 2$  amplitudes dominate, corresponding to  $(\lambda_1, \lambda_2) = (\pm, \mp)$ .

### C. Amplitudes for $Z$ boson decay to leptons

The decay helicity amplitude for the  $1 \rightarrow 2$  process such as  $Z \rightarrow \ell\bar{\ell}$  is essentially a matrix element of the spin-1 rotation matrix, which is the inner product between states with definite projections of angular momenta along a chosen axis [19]. We have defined our angles, in particular  $\theta_1, \theta_2, \phi_1$ , and  $\phi_2$ , such that we need consider only  $Z_i(\lambda) \rightarrow \ell_\sigma(\theta_i, \phi_i)\bar{\ell}_{\bar{\sigma}}$ . That is, the amplitude has the same form for  $i = 1$  and for  $i = 2$ . Specifically, following the conventions described above in Eq. (28) and (33), we find that

$$\mathcal{M}_{\lambda_i; \sigma_i \bar{\sigma}_i}^{(i)} = \Delta\sigma_i (-1)^{\lambda_i} \sqrt{2} g_{\Delta\sigma}^{Z\ell\bar{\ell}} d(\Delta\sigma_i, \lambda_i, \theta_i) m_i e^{i\lambda_i\phi_i}, \quad (44)$$

where  $d(\Delta\sigma_i, \lambda_i, \theta_i) = d_{\Delta\sigma_i, \lambda_i}^{\max(|\Delta\sigma_i|, |\lambda_i|)}(\theta_i)$  in the conventions of Ref. [23]. In the above,  $m_i$  is the invariant mass of  $Z_i$ ,  $\lambda_i$  is its helicity,  $\Delta\sigma_i = \sigma_i - \bar{\sigma}_i$ , and the coupling of the  $Z$  to the lepton pair is

$$g_{\Delta\sigma}^{Z\ell\bar{\ell}} = \frac{|e|(T_3 + \sin^2\theta_W)}{\sin\theta_W \cos\theta_W}, \quad (45)$$

where  $T_3 = -1/2$  (0) for left (right)-handed leptons. Note that the amplitude in Eq. (44) vanishes for  $\Delta\sigma_i = 0$  in the limit of massless leptons, which is the limit taken in this work. For  $\Delta\sigma_i = -1$ , the expression in Eq. (44) reproduces Eq. (4.8a) in Ref. [17].

### D. Differential cross sections for signal and background

The full amplitude of  $q\bar{q} \rightarrow Z_1 Z_2 \rightarrow (\ell_1 \bar{\ell}_1)(\ell_2 \bar{\ell}_2)$  is then

$$\mathcal{M}(\sigma, \bar{\sigma}; \sigma_i) = \sum_{\lambda_1, \lambda_2} \mathcal{M}_{\sigma\bar{\sigma}; \lambda_1 \lambda_2}^{ZZ} D_Z(k_1^2) D_Z(k_2^2) \mathcal{M}_{\lambda_1; \sigma_1 \bar{\sigma}_1}^{(1)} \mathcal{M}_{\lambda_2; \sigma_2 \bar{\sigma}_2}^{(2)}, \quad (46)$$

where the propagator factor for the  $Z$  boson may be taken to be

$$D_Z(q^2) = \frac{1}{q^2 - m_Z^2 + im_Z\Gamma_Z}. \quad (47)$$

The full differential cross section is then (using the short-hand notation  $\Omega = \{\Theta, \theta_1, \theta_2, \phi_1, \phi_2\}$  and  $d\Omega = d\cos\Theta d\cos\theta_1 d\cos\theta_2 d\phi_1 d\phi_2$ )

$$\frac{d\sigma}{d\Omega dm_1^2 dm_2^2} = 2\pi \frac{1}{4} \frac{1}{3} \frac{1}{2\hat{s}} \frac{\beta_1(1+x)}{32\pi^2} \left(\frac{1}{32\pi^2}\right)^2 \left(\frac{1}{2\pi}\right)^2 \sum_{\sigma, \bar{\sigma}, \sigma_i} |\mathcal{M}(\sigma, \bar{\sigma}; \sigma_i)|^2, \quad (48)$$

where  $2\pi$  comes from integrating over the unobservable production azimuthal angle,  $1/4$  from averaging over initial spin states,  $1/3$  from averaging initial color states,  $1/(2\hat{s})$  from the incoming flux,  $\beta_1(1+x)/(32\pi^2)$  from the  $ZZ^{(*)}$  two-body phase space,  $1/(32\pi^2)$  from the phase space of each of the  $\ell\bar{\ell}$  final states, and  $1/(2\pi)$  from each  $dm_i^2$  integral that one obtains when re-expressing the four particle phase space in terms of the  $dm_i^2$  variables (see for example [24]).

Likewise, in the case of the  $gg \rightarrow h \rightarrow Z_1 Z_2 \rightarrow (\ell_1 \bar{\ell}_1)(\ell_2 \bar{\ell}_2)$  signal, the full amplitude is

$$\mathcal{M}(h; \sigma_i) = \sum_{\lambda_1, \lambda_2} \mathcal{M}_{h; \lambda_1 \lambda_2}^{ZZ} D_Z(k_1^2) D_Z(k_2^2) \mathcal{M}_{\lambda_1; \sigma_1 \bar{\sigma}_1}^{(1)} \mathcal{M}_{\lambda_2; \sigma_2 \bar{\sigma}_2}^{(2)}, \quad (49)$$

and the full differential cross section is

$$\frac{d\sigma}{d\Omega dm_1^2 dm_2^2} = 2\pi \frac{1}{4} \frac{1}{8} \frac{1}{2\hat{s}} \frac{\beta_1(1+x)}{32\pi^2} \left(\frac{1}{32\pi^2}\right)^2 \left(\frac{1}{2\pi}\right)^2 \binom{2}{\sigma_i} \sum_{\sigma_i} |\mathcal{M}(h; \sigma_i)|^2. \quad (50)$$

Note that the only significant difference between Eq. (48) and Eq. (50) is that color averaging yields a factor of  $\frac{1}{3}$  in Eq. (48), but  $\frac{1}{8}$  in Eq. (50). The factor of 2 before the sum in Eq. (50) is from summing over initial gluon helicities.

Before proceeding, we note our definitions of  $Z_1$  and  $Z_2$ . When the two  $Z$  bosons decay into  $2e2\mu$  final states, we define  $Z_1$  to be the parent particle of the electron/positron pair, while for  $4e$  or  $4\mu$  final states,  $Z_1$  is the  $Z$  with lower invariant mass. Technically, one could reconstruct e.g. a  $4\mu$  final state in two ways (in terms of assigning a particular muon and a particular antimuon to a given  $Z$ ), however generally one of these reconstructions would make the resulting  $Z$ s far off-shell. Hence we only keep the reconstruction for which the product of the  $Z$  Breit-Wigner factors is largest. We note that the total event rate of  $ZZ^{(*)} \rightarrow 2e2\mu$  is a factor of two larger than that of  $ZZ^{(*)} \rightarrow 4e$  or  $ZZ^{(*)} \rightarrow 4\mu$ .

## E. Angular distributions

Analytic expressions for the background and signal distributions are contained in Eqs. (48) and (50). However, they are too long to be presented explicitly and not very illuminating.

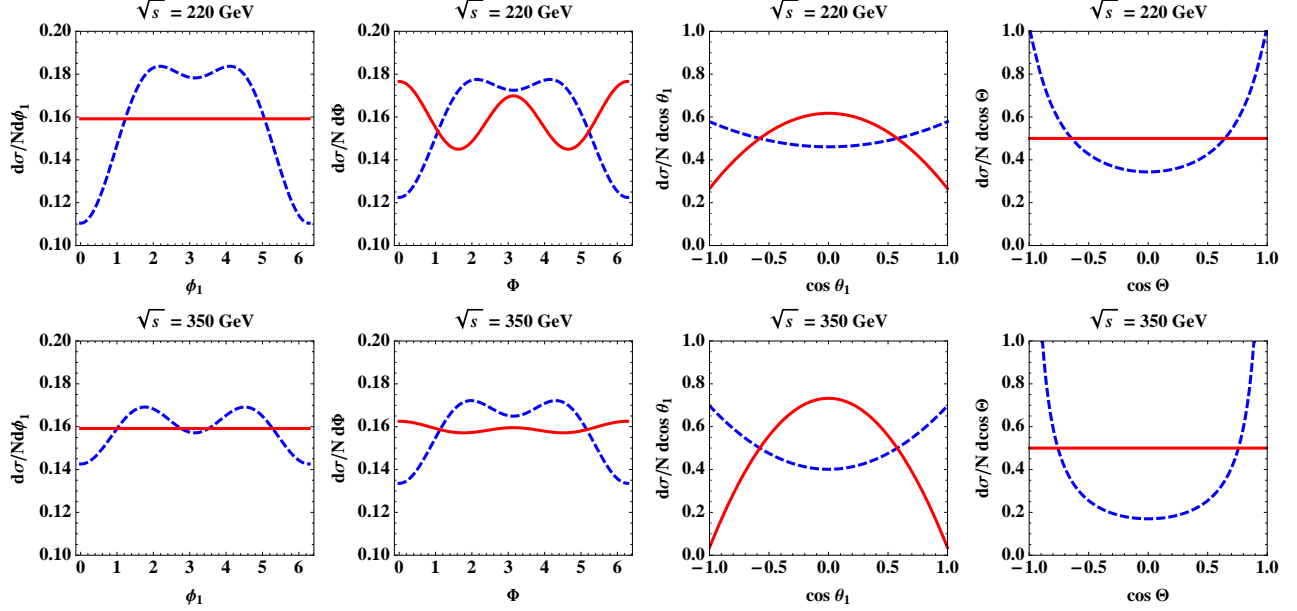


FIG. 3: *Signal and background singly differential distributions at  $m_h = \sqrt{s} = 220$  and  $350$  GeV. The blue (dashed) lines are background distributions and the red (solid) lines are signal distributions.*

Instead we will show figures for all the singly and doubly distributions for the signal and the background in this subsection.

In Fig. 3 we show normalized singly differential distributions in  $\phi_1$ ,  $\Phi \equiv \pi - \phi_1 - \phi_2$ ,  $\Theta$ , and  $\theta_1$  for the processes  $u\bar{u} \rightarrow ZZ \rightarrow 4\ell$  and  $h \rightarrow ZZ \rightarrow 4\ell$  at  $m_h = \sqrt{s} = 220$  and  $350$  GeV. (For simplicity, we take the  $Z$  bosons to be on-shell.) One notable feature is that the signal  $\phi_1$  distribution is flat, although there are correlations between  $\phi_1$  and  $\phi_2$  such that  $\Phi$  exhibits a  $\cos 2\Phi$  dependence. It was pointed out in Refs. [12, 13] that this observable is very useful in discerning the spin and CP properties of a singly produced resonance decaying to two  $Z$  bosons. In addition, distributions in the production angle  $\Theta$  indicate that the  $ZZ$  pair produced by the background process tend to be in the forward region inside the detector; this is especially pronounced when the invariant mass is high. This is a feature of the  $t$ -channel production mechanism which has been suggested as a way to tag the vector boson fusion production of the Higgs boson, where there are two forward jets in the event. In the signal case, on the contrary, the  $Z$ s are produced isotropically, as expected from the fact that the Higgs is a scalar particle.

It is also interesting to consider doubly differential angular distributions for signal and background, which are shown in Fig. 4. We plot distributions in the following pairs of angles:

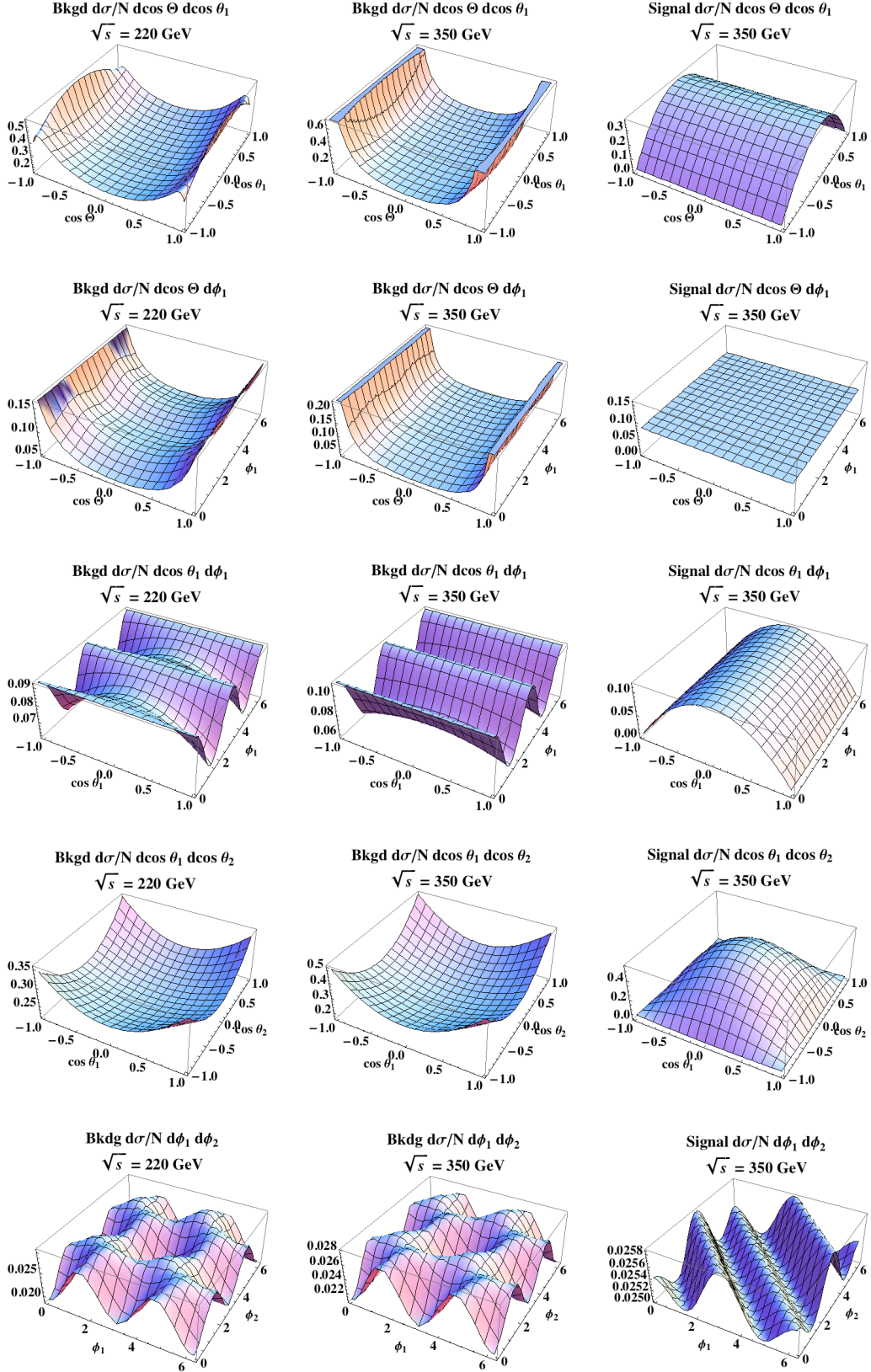


FIG. 4: Doubly differential distributions for signal and background. See the text for more explanations.

$(\Theta, \theta_1)$ ,  $(\Theta, \phi_1)$ ,  $(\theta_1, \phi_1)$ ,  $(\theta_1, \theta_2)$ , and  $(\phi_1, \phi_2)$ . The background distributions are again from  $u\bar{u}$  initial states and shown for  $\sqrt{s} = 220$  and 350 GeV. We observe noticeable changes in the distributions of the first three pairs of variables for these two different center-of-mass energies. On the other hand, the signal distributions do not change as much when one varies the Higgs mass, except for the  $(\phi_1, \phi_2)$  distributions, and are shown only for  $m_h = 350$  GeV. The background exhibits strong correlations between the pairs of angles in all five cases.

#### IV. STATISTICAL PROCEDURES

Likelihood methods are frequently employed to establish the presence, or lack, of a signal using kinematic distributions which discriminate signal from background. For example, if the purpose is discovery, one considers the “null hypothesis” assuming the observed data set is entirely due to background and an “alternative hypothesis” assuming the presence of both signal and background. A likelihood function is defined for each hypothesis to quantify the probability of obtaining the actual data under that particular hypothesis. In order to accept or reject one hypothesis in favor of the other, a “test statistic” must also be defined.

In quantum field theory there is a natural object quantifying the probability of obtaining a particular event in a given set of data: the differential cross section. This motivates the use of the MEM, which is simply the use of likelihood methods where the probability density function (pdf) used in the likelihood is the properly normalized differential cross section (or “matrix element”) with respect to certain kinematic variables<sup>1</sup>. When the number of events is small one can include every event in the evaluation of the likelihood. This “unbinned likelihood method” is what we adopt in the following.

##### A. Extended maximum likelihood method

When there exist free parameters in the underlying hypothesis one wishes to test<sup>2</sup>, statistically preferred values of the parameters of the underlying model are found by maximizing the likelihood function with respect to those parameters. When the overall number of events is not fixed but allowed to fluctuate, the normalization of the likelihood function may become

---

<sup>1</sup> We use “pdf” for probability density function and “PDF” for parton distribution function.

<sup>2</sup> In such cases the hypothesis is called “composite”, while those without free parameters are called “simple”.



a free parameter. In this case, one is using the “extended” maximum likelihood method [25], which we employ in this work.

To be more specific, we consider the likelihood for some collider signature with (unknown) expected number of events  $\mu$  described by kinematic information  $\mathbf{x} = \{x_1, x_2, \dots, x_N\}$ , where the  $x_i$  are kinematic variables describing event  $i$  of  $N$  total events. The unbinned likelihood is simply

$$\mathcal{L}(\mu; \boldsymbol{\theta}) = \frac{e^{-\mu} \mu^N}{N!} \prod_{i=1}^N P(\boldsymbol{\theta}; x_i), \quad (51)$$

where  $P(\boldsymbol{\theta}; x)$  is the pdf for the kinematic variables as a function of  $\boldsymbol{\theta}$ , the parameters of the underlying model. In the MEM,  $P(\boldsymbol{\theta}, x)$  is the differential cross section normalized by the total cross section, generally scaled by efficiencies and acceptances of the detector involved.

We will define  $P_s(m_h, x_i)$  to be the normalized pdf for the signal process, which depends on one underlying parameter, the Higgs mass  $m_h$ .<sup>3</sup> The normalized pdf for the background process is then given by  $P_b(x_i)$ ; it is assumed here that the differential cross section for the background process is known and contains no unknown parameters. The likelihood function for the signal plus background hypothesis is then given by

$$\mathcal{L}_{s+b}(\mu, f, m_h) = \frac{e^{-\mu} \mu^N}{N!} \prod_{i=1}^N [f P_s(m_h; x_i) + (1 - f) P_b(x_i)], \quad (52)$$

where  $\mu = \mu_s + \mu_b$  is the sum of the expected number of signal events  $\mu_s$  and expected number of background events  $\mu_b$ , while the signal fractional yield  $f$  is defined as

$$0 < f = \frac{\mu_s}{\mu_s + \mu_b} < 1. \quad (53)$$

We often refer to  $f$  simply as the “yield”. For  $\mathcal{L}_b$ , the likelihood for the background-only hypothesis, we simply set  $\mu_s = 0$ . When computing the likelihood for each hypothesis, we calculate the maximum of  $\mathcal{L}_{s+b}$  in  $\{\mu, m_h, f\}$  and  $\mathcal{L}_b$  in  $\mu$ , respectively<sup>4</sup>. In practice, since the Poisson distribution factors in the definition of the likelihood function, the maximum of the likelihood always occurs at  $\mu = N$ . So effectively one can replace  $\mu$  by  $N$ , the measured total number of events, in the calculation.

<sup>3</sup> We set the Higgs width to the SM value for the given Higgs mass,  $m_h$ , as found by HDECAY [26].

<sup>4</sup> In our fitting procedure, we look for the local maximum closest to the true Higgs mass.

## B. Expected significance

In determining the significance for Higgs discovery from a set of events, we are really comparing the likelihood of two hypotheses: (i) that the events consist of signal events from the Higgs boson at some mass, as well as events from background  $q\bar{q} \rightarrow ZZ^{(*)}$  production, and (ii) that all the events are due to  $q\bar{q} \rightarrow ZZ^{(*)}$  production. Our choice of test statistic for describing this relative likelihood is the likelihood ratio

$$\mathcal{Q} = \frac{\mathcal{L}_{s+b}}{\mathcal{L}_b}, \quad (54)$$

from which the significance of discovery is computed

$$\mathcal{S} = \sqrt{2 \ln \mathcal{Q}}. \quad (55)$$

This test statistic was used by the LEP experiments in their Higgs searches [27], while its use for  $h \rightarrow ZZ^{(*)} \rightarrow 4\mu$  was studied in Ref. [28]. In our case we include the angular correlations in the likelihood function. The expected significance  $\mathcal{S}$  is then obtained by performing a large number of pseudo-experiments and choosing the median value. The 1 and 2  $\sigma$  spreads in  $\mathcal{S}$  are determined from the distribution of significances obtained from the pseudo-experiments.

## C. Exclusion limit

We determine the exclusion limit, in the absence of a signal, by setting an upper limit on the yield,  $f$ , defined in Eq. (53). For a particular choice of Higgs mass  $\hat{m}_h$ , we define a pdf  $p(f)$  by considering the likelihood  $\mathcal{L}_{s+b}$  as a function of  $f$ ,

$$p(f) = \frac{\mathcal{L}_{s+b}(N, f, \hat{m}_h)}{\int_0^1 \mathcal{L}_{s+b}(N, \bar{f}, \hat{m}_h) d\bar{f}}. \quad (56)$$

The 95% confidence level limit on  $f$  for a given set of data is given by  $\alpha$  as follows:

$$\int_0^\alpha p(f) df = 0.95. \quad (57)$$

We then translate  $\alpha$  into a 95% confidence level upper limit on the Higgs production cross section by unfolding with the detector acceptances and efficiencies. The expected exclusion limit is obtained by performing a large number of pseudo-experiments.

It should be noted that the procedure above for setting the exclusion limit only takes into account differences in the shape of kinematic distributions between signal and background.

In particular we are mainly interested in possible improvements by including angular distribution in addition to the invariant mass spectrum. Typically experimental collaborations set limits directly on the normalization of the signal cross section by performing counting experiments in a particular window of total invariant mass. In comparison with the standard  $CL_s$  method employed by ATLAS and CMS collaborations, our method should be considered as a shortcut for the purpose of understanding the improvement from incorporating the angular correlations. One would hope to incorporate both the counting experiments and shape measurements in a more complete study.

#### D. Probability density functions

In this subsection we define the signal and background pdfs that enter into the likelihood function in Eq. (52). The kinematic observables are  $\mathbf{x} = \{Y, \hat{s}, m_1^2, m_2^2, \Omega\}$ , where  $Y$  is the pseudo-rapidity of the  $ZZ^{(*)}$  system,  $\hat{s}$  is the partonic center-of-mass energy,  $m_{1(2)}$  is the invariant mass of the  $Z_{1(2)}$  boson, and  $\Omega$  represents the production and decay angles.

The signal pdf is

$$P_s(m_h; \mathbf{x}) = \frac{1}{\epsilon_s \sigma_s(m_h)} \frac{d\sigma_s(m_h; \mathbf{x})}{dY d\hat{s} dm_1^2 dm_2^2 d\Omega}, \quad (58)$$

where  $\sigma_s(m_h)$  is the total hadronic cross section,  $d\sigma_s$  is the corresponding differential cross section, and  $\epsilon_s$  is the total signal efficiency (which in principle includes geometric acceptance as well as reconstruction efficiencies). More explicitly,

$$P_s(m_h; \mathbf{x}) = \frac{1}{\epsilon_s \sigma_s(m_h)} \left( \frac{f_g(x_1) f_g(x_2)}{s} \right) \frac{d\hat{\sigma}_h(m_h, \hat{s}, m_1, m_2, \Omega)}{dm_1^2 dm_2^2 d\Omega}. \quad (59)$$

In the above,  $\hat{\sigma}_h$  is the partonic cross section, and the  $f_g(x)$  is the gluon PDF.

For the background pdf we take into account the fact that, in a hadron collider, we are unable to determine the direction of the initial quark (as opposed to the anti-quark) on an event-by-event basis by calculating the cross section for each choice of initial quark direction and summing the two. This may be written as

$$P_b(\mathbf{x}) = \frac{1}{\epsilon_b \sigma_{q\bar{q}}} \left( \left( \frac{f_q(x_1) f_{\bar{q}}(x_2)}{s} \right) \frac{d\hat{\sigma}_{q\bar{q}}(\hat{s}, m_1, m_2, \Omega)}{dm_1^2 dm_2^2 d\Omega} + \left( \frac{f_{\bar{q}}(x_1) f_q(x_2)}{s} \right) \frac{d\hat{\sigma}_{q\bar{q}}(\hat{s}, m_1, m_2, \Omega')}{dm_1^2 dm_2^2 d\Omega'} \right), \quad (60)$$

where  $\Omega' \equiv (\pi - \Theta, \theta_1, \theta_2, \phi_1 + \pi, \phi_2 + \pi)$  is the shift in angles needed for an initial quark in the  $-z$  direction and we have switched the quark PDF with the anti-quark PDF (or

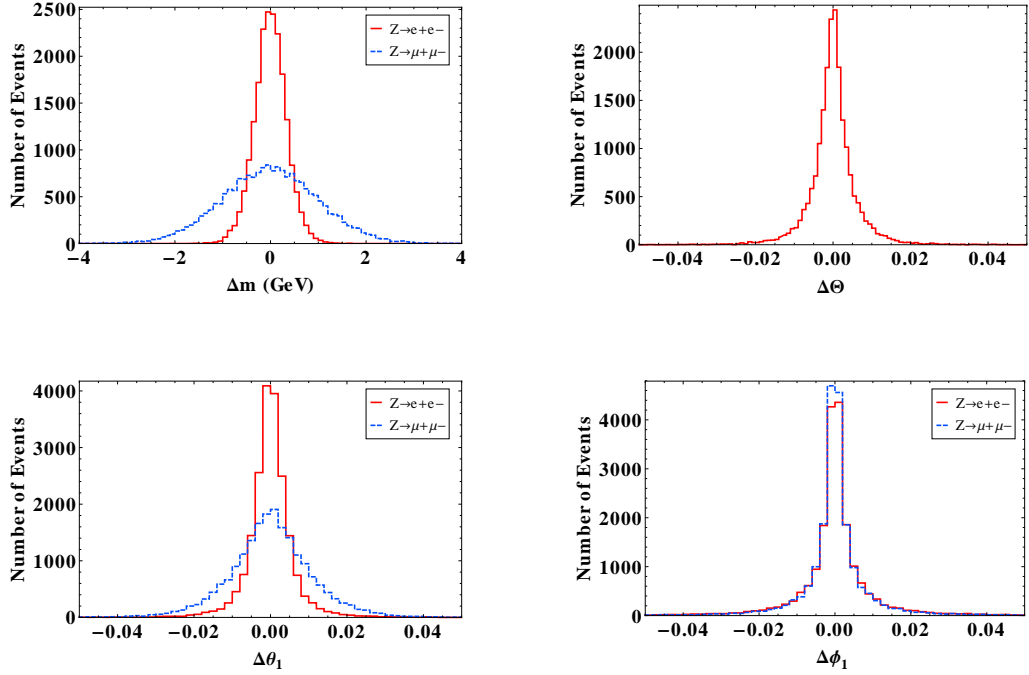


FIG. 5: *Effect of detector resolution in measuring  $E$  and  $p_T$  on kinematic variables. Each of the histograms were generated using twenty thousand events. The channel used for these plots is the background  $2e2\mu$  channel.*

equivalently switched  $x_1$  and  $x_2$ ). The total  $q\bar{q} \rightarrow ZZ^* \rightarrow 4\ell$  cross section is given by  $\sigma_{q\bar{q}}$  with the function  $f_{q(\bar{q})}$  representing the quark (anti-quark) PDF, and  $\epsilon_b$  the total efficiency for this channel. In calculating the cross section,  $\hat{\sigma}_{q\bar{q}}$ , for the  $q\bar{q} \rightarrow ZZ^{(*)} \rightarrow 4\ell$  background, we sum over the quark flavors,  $u, d, s$  and  $c$ . We use CTEQ5L for the PDFs indicated in Eq. (59) and Eq. (60) as  $f_i(x)$  [29].

## V. MONTE CARLO SIMULATIONS

We generate the signal and background events for our analysis using MadGraph/MadEvent (MG/ME) version 4.4.52 [30]. Proton-proton collisions at  $\sqrt{s} = 7$  TeV are implemented with the CTEQ5L [29] PDFs. As noted above, the main irreducible background, and the only one which we will consider in our analysis, is  $q\bar{q} \rightarrow ZZ^{(*)} \rightarrow 4\ell$ . For signal we consider only  $gg \rightarrow h \rightarrow ZZ^{(*)} \rightarrow 4\ell$ , without additional jets in the final states; effectively our analysis considers only the “0-jet bin” for the  $ZZ^{(*)} \rightarrow 4\ell$  channel.

Detector effects are modeled by applying Gaussian smearing to the energy of electrons according to

$$\left(\frac{\sigma_{E,e}}{E}\right)^2 = \left(\frac{0.036}{\sqrt{E}}\right)^2 + 0.0026^2, \quad (61)$$

and to the  $p_T$  of muons according to

$$\sigma_{p_T,\mu} = 0.015 p_T - 5.710^{-6} p_T^2 + 2.210^{-7} p_T^3. \quad (62)$$

These expressions follow the CMS TDR [31]. The value of the constant term in Eq. (61) may be somewhat optimistic. However, we verified that our results do not change significantly when using a value for this quantity that is twice as large. The smearing of the muon  $p_T$  is quite conservative as we have used the resolution corresponding to  $1.8 < |\eta| < 2.0$  and assumed this to be the same for lower values of  $\eta$  as well. The angles measured in the lab frame are not smeared. Nevertheless, angles which define the kinematics of the four lepton system, as described in Sect. II, are affected by the  $E$  and  $p_T$  resolution, as can be seen in Fig. 5. A more sophisticated treatment of detector effects would include the effects of reconstruction efficiencies, which we neglect for simplicity.

Another effect of smearing the lepton  $E$  or  $p_T$  is that the four lepton system will now have a small  $p_T$  in the lab frame, even without the presence of additional jets or particles in the final states. We simply boost away this induced  $p_T$  and proceed to define angles as in Section II.

After generating events and smearing the lepton  $p_T$ , we apply the following cuts to each of the lepton in the lab frame:

$$\begin{aligned} |p_T| &\geq 10 \text{ GeV} , \\ |\eta| &\leq 2.5 . \end{aligned}$$

Moreover, we focus on the following window for the  $4\ell$  invariant mass

$$150 \text{ GeV} \leq \hat{s} \leq 450 \text{ GeV} . \quad (63)$$

The efficiency (geometric acceptance) for our selection of signal events is listed in Table I and varies from  $\sim 0.5$  to  $\sim 0.7$  as we increase the mass of the Higgs boson from 170 GeV to 350 GeV. The efficiency for selection of background events is 0.52. Moreover, these cuts affect the reconstructed angular distributions. As can be seen in Fig. 6, the distributions

	$m_h(\text{GeV})$	$\sigma(\text{fb})$	$\epsilon$	$\langle N \rangle$
Signal	175	0.218	0.512	0.279
	200	1.26	0.594	1.87
	220	1.16	0.625	1.81
	250	0.958	0.654	1.57
	300	0.714	0.701	1.25
	350	0.600	0.708	1.06
Background	-	8.78	0.519	11.4

TABLE I: *Expected number of events  $\langle N \rangle$  for the signal and background  $2e2\mu$  channel at  $2.5\text{fb}^{-1}$ . The SM cross section without any cuts is denoted by  $\sigma$ , while  $\epsilon$  is the efficiency of our analysis cuts. The  $4e$  and  $4\mu$  channel yields are half of the  $2e2\mu$  channel and their efficiencies are the same as the  $2e2\mu$  channel.*

with respect to  $\Theta$ ,  $\phi_1$  and  $\phi_2$  are modified most significantly by our acceptance cuts. In the case of the  $\Theta$  distribution it is easy to see that the loss of events in the forward region due to  $p_T$  and rapidity cuts cause a change in the shape of the distribution. The  $\phi_1$  and  $\phi_2$  distributions undergo less trivial modifications.

Also listed in Table I are the cross sections and expected number of events after selection cuts, with an integrated luminosity of  $2.5\text{fb}^{-1}$ , for both signal and background at the LHC with  $\sqrt{s} = 7\text{TeV}$ . The cross sections for the signal and background processes are obtained from MG/ME with  $K$ -factors applied. As we are considering the 0-jet bin for signal and background, there are a number of complications in determining the appropriate higher order cross section [32], a complete study of which is beyond the scope of this paper. Therefore we simply apply a  $K$ -factor of 1.5 for the signal and a  $K$ -factor of 1.33 for the background. (The  $K$ -factor for the background is the value obtained in Ref. [33].) We note that these  $K$ -factors, are not used in the analyses themselves, but only in determining the number of events of each type to include in the pseudo-experiments.

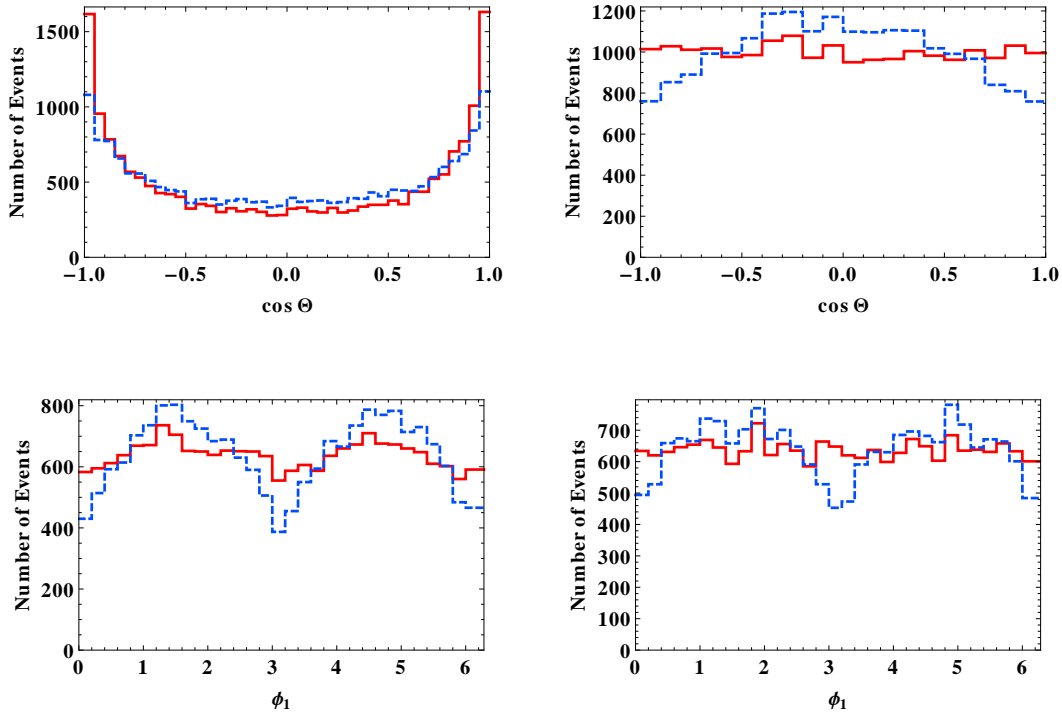


FIG. 6: *The effect on  $\cos \Theta$  and  $\phi_1$  distributions from rapidity and transverse momentum cuts on final state leptons. The panels on the left show the distribution for background events before (red) and after (blue) the cuts. The panels on the right show the distributions for signal events before (blue) and after (red) the cuts. Signal distributions correspond to a SM Higgs boson with  $m_h = 300$  GeV.*

## VI. RESULTS

In this section we present our results for the expected significance and expected exclusion limits from the MEM, which includes the following kinematic variables for the four lepton final state,

$$\mathbf{x} = \{Y, \hat{s}, m_1^2, m_2^2, \Theta, \theta_1, \theta_2, \phi_1, \phi_2\}. \quad (64)$$

For comparison we also present results from an analogous analysis, which uses only invariant mass information in the pdf. (Specifically we consider the product of Breit-Wigner factors for the Higgs as our signal pdf and use the invariant mass distribution from simulated data as the background pdf.) Our results are for the LHC at  $\sqrt{s} = 7$  TeV and integrated luminosities of 2.5, 5, and 7.5  $\text{fb}^{-1}$  for discovery and 1, 2.5, and 5  $\text{fb}^{-1}$  for exclusion.

## A. Expected significance

To compute the expected significance, we perform ten thousand pseudo-experiments (each) for Higgs masses of 175, 200, 220, 250, 300, and 350 GeV. Each pseudo-experiment consists of signal and background events with  $4\mu$ ,  $2e2\mu$ , and  $4e$  final states; the number of events of each type are chosen from Poisson distributions, where the expected numbers of signal and background events are given by the product of the luminosity under consideration, the theoretical cross section, and acceptance efficiencies after smearing and cuts. The cross section after cuts is also used to normalize the signal and background pdfs  $P_s$  and  $P_b$  in the likelihood function in Eq. (52). As we do not include the different reconstruction efficiencies for electrons and muons in our analysis,  $P_s$  and  $P_b$  are identical for  $4\mu$ ,  $2e2\mu$ , and  $4e$  final states. However, we do consider the yields in each channel as separate parameters when finding the significance from pseudo-experiments by maximizing the likelihood with respect to the undetermined parameters.

The median values of significance obtained for each Higgs mass in this channel, using both the MEM (all kinematic variables) and the likelihood method (invariant mass only), are shown in Fig. 7. The  $1\sigma$  and  $2\sigma$  bands on the significance obtained from the MEM are also shown in this figure. We do not show the corresponding bands for the invariant mass-based analysis; the widths of the bands for this case are similar.

We note that the MEM consistently outperforms the invariant mass only method, and that the effect is more pronounced, on the order of 10 - 20 %, at higher Higgs masses. This is because the helicity amplitudes for  $h \rightarrow ZZ^{(*)}$  and  $q\bar{q} \rightarrow ZZ^{(*)}$  are increasingly different at larger values of invariant mass. More specifically, as already pointed out in Sect. III, the  $(\lambda_1, \lambda_2) = (\pm 1, \mp 1)$  amplitudes dominate in the high mass case for  $q\bar{q}$ , while only the  $(\lambda_1, \lambda_2) = (0, 0)$  amplitude survives in the heavy Higgs limit in the  $h \rightarrow ZZ^{(*)}$  case.

## B. Exclusion

In Figure 8, we show the median 95% confidence level exclusions on the yield parameter  $f$ , both as obtained with the MEM and as obtained with a likelihood method using only invariant mass information. These limits were obtained using the procedure described in Subsection IV C to find the 95% confidence limit on  $f$  in a given pseudo-experiment consist-



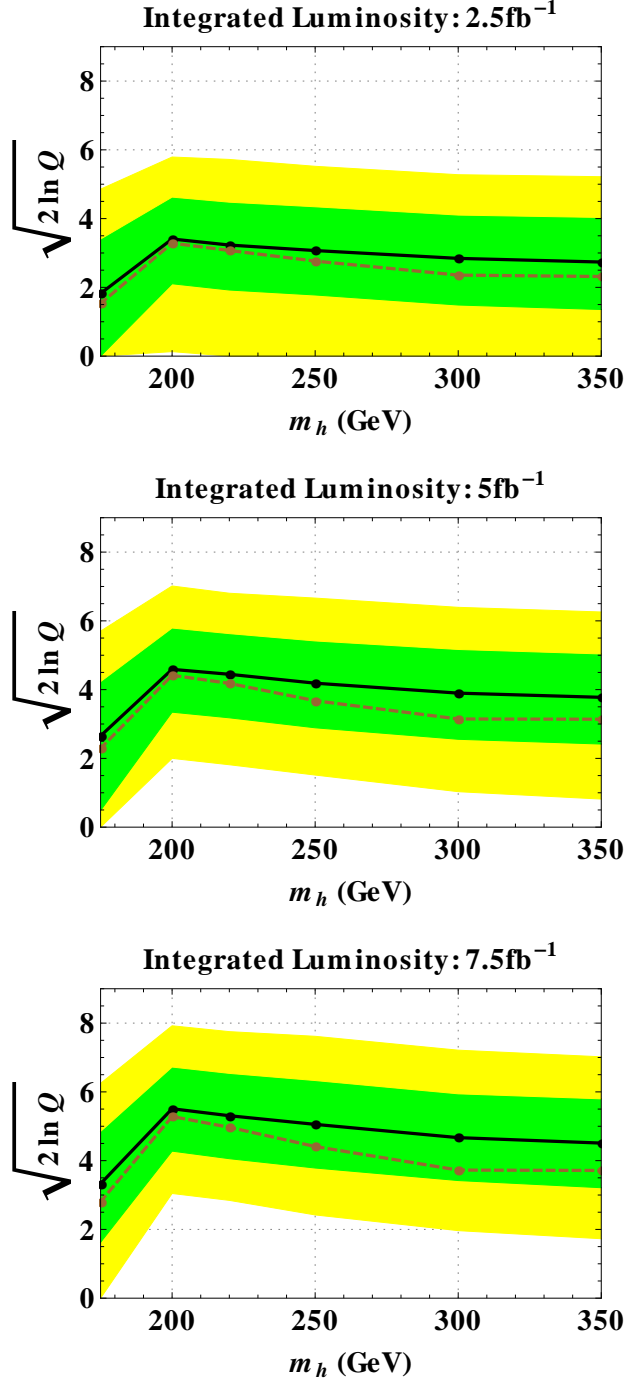


FIG. 7: Comparison of significance for Higgs discovery obtained from using only invariant mass information (brown dotted line) with that obtained from all of the kinematic variables using the MEM (black solid line) at different integrated luminosities. The green and yellow bands correspond to less than  $1$  and  $2 \sigma$  deviations from the median expected significance in the case where we use all kinematic variables.

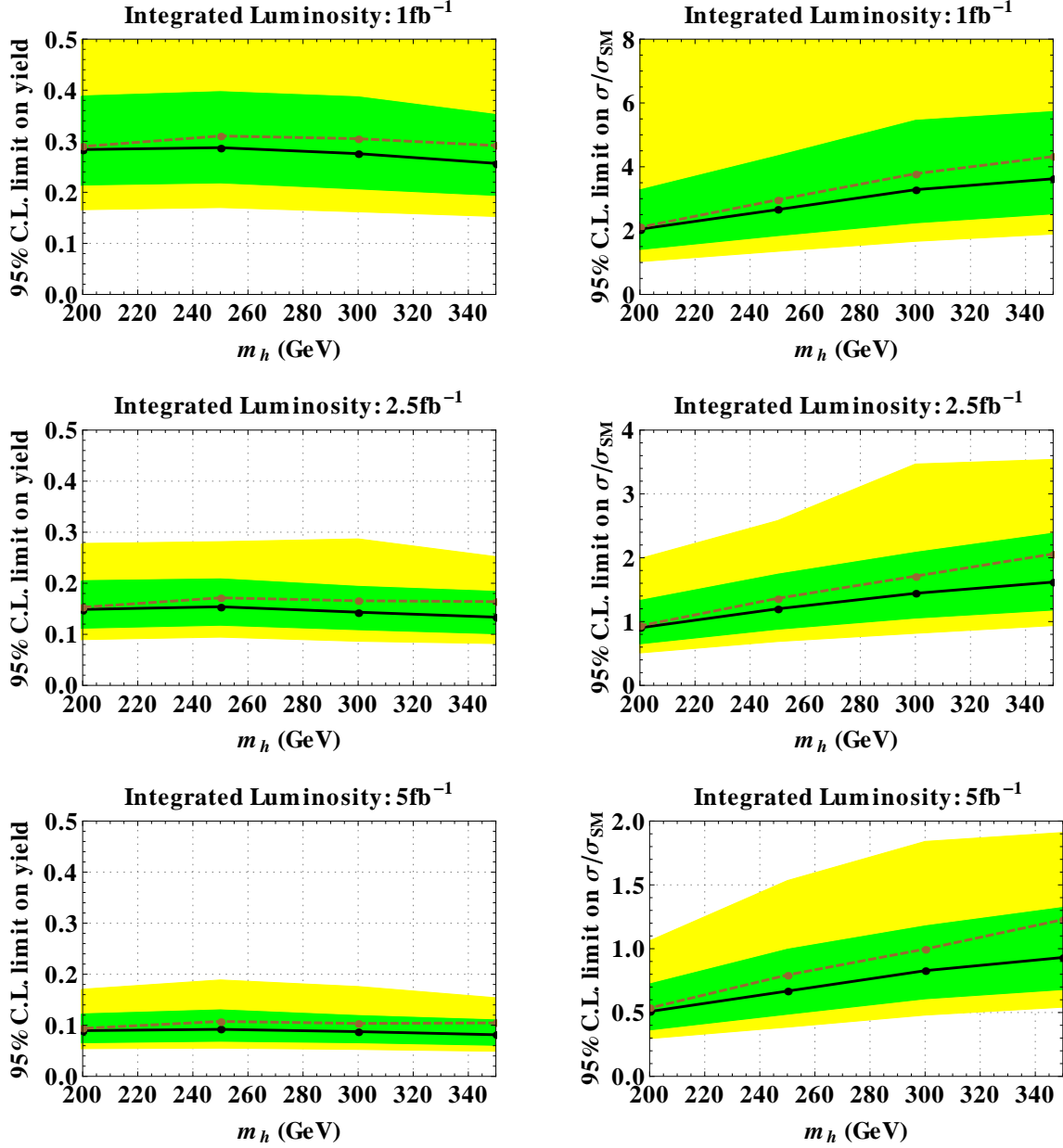


FIG. 8: The panels on the left contain 95% confidence level exclusion limits on the Higgs signal yield,  $f$ , while the panels on the right contain these limits interpreted as limits on the Standard Model Higgs cross section. The exclusions represented by the brown, dashed line were obtained using only the invariant mass distribution, while all of the kinematic variables were used (via the MEM) in obtaining those exclusions represented by the black solid line. The green and yellow bands correspond to less than 1 and 2  $\sigma$  deviations from the median expected exclusion in the case where we use all kinematic variables. These results were obtained by performing one thousand pseudo-experiments.

ing only of background events, which were generated, as in our investigation of significance, using the method described in Section V. We note that in obtaining these limits, the yield,  $f$ , was fixed to be the same for each of the three channels ( $4e$ ,  $2e2\mu$ , and  $4\mu$ ), and one thousand pseudo-experiments were performed.

We can translate a limit on the yield to a limit on the Higgs production cross section, since the yield is defined as the ratio of the expected number of signal events to the expected number of signal and background events. As this is the expected number of events after the selection cuts are applied, it is proportional to the cross section times efficiency, rather than simply the cross section. Specifically, we find

$$\sigma_s = \left(\frac{\epsilon_b}{\epsilon_s}\right) \left(\frac{f}{1-f}\right) \sigma_b, \quad (65)$$

where  $\epsilon_{s(b)}$  and  $\sigma_{s(b)}$  are the signal (background) efficiency and cross section respectively. Eq. (65) allows us to translate our limits on  $f$  into a limit on  $\sigma_s$ , the Higgs cross section, as is done in Fig. 8. For simplicity we do not include any systematic uncertainties (e.g. on the efficiencies) in the analysis. We see that, as in the investigation of significance considered above, the difference in sensitivity between the MEM and the invariant-mass-only analysis is greater in the higher Higgs mass range.

## VII. CONCLUSIONS

Traditional search strategies for the Higgs boson in the  $ZZ^{(*)} \rightarrow 4\ell$  channel concentrate only on measurements of the total invariant mass of the four leptons. Since the four-momenta of all final state particles can be reconstructed, we have considered in this work the possibility of including all available kinematic information in discriminating the Higgs signal from the dominant irreducible background at the LHC with  $\sqrt{s} = 7$  TeV, by implementing the Matrix Element Method.

We first derived Lorentz-invariant expressions for the production and decay angles used in the analyses, which allow for reconstruction of these angular variables from momenta measured in the laboratory frame. Then we presented analytic expressions for the fully differential distributions for both signal and background, allowing the  $Z$  bosons to be off-shell.

We found that greater sensitivity in discovering or excluding the Standard Model Higgs

boson can be achieved when including spin correlations in addition to total invariant mass measurements. Generally, these improvements are on the order of 10 - 20 %; they are larger for higher Higgs masses, for which the differences between signal and background distributions are greater.

Searching for the Higgs boson is among the top priorities of the physics program at the LHC. Our results indicate it would be worthwhile to include full angular distributions in actual experimental searches in the golden channel through some type of multivariate analyses. Whether a Standard Model Higgs boson will be discovered or excluded in the near future, we eagerly await the result!

### Acknowledgments

We would like to thank Johan Alwall, Pierre Artoisenet, Pushpa Bhat, Qinghong Cao, Johannes Heinonen, Wai-Yee Keung, Jen Kile, Andrew Kobach, Andrew Kubik, Tom LeCompte, Joe Lykken, Olivier Mattelaer, Frank Petriello, Seth Quackenbush, Heidi Schellman, Michael Schmitt, Shashank Shalgar, Gabe Shaughnessy, Tim Tait, and Nhan Tran for useful conversations and/or correspondence. RVM acknowledges the support of a GAANN fellowship. This work was supported in part by the U.S. Department of Energy under contract numbers DE-AC02-06CH11357 and DE-FG02-91ER40684.

- 
- [1] A. Djouadi, Phys. Rept. **457**, 1 (2008) [arXiv:hep-ph/0503172].
  - [2] The CDF, D0 Collaborations, the Tevatron New Phenomena, Higgs Working Group. arXiv:1107.5518 [hep-ex].
  - [3] ATLAS Collaboration, “Combined Standard Model Higgs Boson Searches in  $pp$  Collisions at  $\sqrt{s} = 7$  TeV with the ATLAS Experiment at the LHC”, ATLAS-CONF-2011-112 (2011).
  - [4] CMS Collaboration, “Search for standard model Higgs boson in  $pp$  collisions at  $\sqrt{s} = 7$  TeV”, CMS-PAS-HIG-11-011 (2011).
  - [5] See, for example, P. C. Bhat, “Advanced analysis methods in particle physics,” FERMILAB-PUB-10-054-E.
  - [6] K. Kondo, J. Phys. Soc. Jap. **57**, 4126 (1988); K. Kondo, J. Phys. Soc. Jap. **60**, 836 (1991);

- K. Kondo, T. Chikamatsu and S. H. Kim, *J. Phys. Soc. Jap.* **62**, 1177 (1993); R. H. Dalitz and G. R. Goldstein, *Phys. Rev. D* **45**, 1531 (1992); R. H. Dalitz and G. R. Goldstein, *Phys. Lett. B* **287**, 225 (1992); G. R. Goldstein, K. Sliwa and R. H. Dalitz, *Phys. Rev. D* **47**, 967 (1993) [arXiv:hep-ph/9205246]; R. H. Dalitz and G. R. Goldstein, *Int. J. Mod. Phys. A* **9**, 635 (1994) [arXiv:hep-ph/9308345]; M. F. Canelli, “Helicity of the  $W$  boson in single - lepton  $t\bar{t}$  events,” FERMILAB-THESIS-2003-22; K. Kondo, *J. Phys. Conf. Ser.* **53**, 202 (2006); P. Artoisenet and O. Mattelaer, *PoS CHARGED2008*, 025 (2008); J. Alwall, A. Freitas and O. Mattelaer, *AIP Conf. Proc.* **1200**, 442 (2010) [arXiv:0910.2522 [hep-ph]]; P. Artoisenet, V. Lemaitre, F. Maltoni and O. Mattelaer, *JHEP* **1012**, 068 (2010) [arXiv:1007.3300 [hep-ph]]; J. Alwall, A. Freitas and O. Mattelaer, *Phys. Rev. D* **83**, 074010 (2011) [arXiv:1010.2263 [hep-ph]]; C. Y. Chen and A. Freitas, *JHEP* **1102**, 002 (2011) [arXiv:1011.5276 [hep-ph]]; I. Volobouev, arXiv:1101.2259 [physics.data-an].
- [7] B. Abbott *et al.* [D0 Collaboration], *Phys. Rev. D* **60**, 052001 (1999) [arXiv:hep-ex/9808029]; V. M. Abazov *et al.* [D0 Collaboration], *Nature* **429**, 638 (2004) [arXiv:hep-ex/0406031]; A. Abulencia *et al.* [CDF Collaboration], *Phys. Rev. D* **74**, 032009 (2006) [arXiv:hep-ex/0605118]; V. M. Abazov *et al.* [D0 Collaboration], *Phys. Rev. D* **78**, 012005 (2008) [arXiv:0803.0739 [hep-ex]]; T. Aaltonen *et al.* [CDF Collaboration], *Phys. Rev. Lett.* **101**, 252001 (2008) [arXiv:0809.2581 [hep-ex]]; F. Fiedler, A. Grohsjean, P. Haefner and P. Schieferdecker, *Nucl. Instrum. Meth. A* **624**, 203 (2010) [arXiv:1003.1316 [hep-ex]]; T. Aaltonen *et al.* [CDF Collaboration], arXiv:1108.1601 [hep-ex].
- [8] CMS Collaboration, “Search for the Higgs Boson in the Fully Leptonic Final State”. CMS-PAS-HIG-11-003 (2011).
- [9] CMS Collaboration, “Search for a Standard Model Higgs boson in the decay channel  $H \rightarrow ZZ^{(*)} \rightarrow 4\ell$ ”, CMS PAS HIG-11-004 (2011).
- [10] T. Matsuura and J. J. van der Bij, *Z. Phys. C* **51**, 259 (1991); S. Y. Choi, D. J. . Miller, M. M. Muhlleitner and P. M. Zerwas, *Phys. Lett. B* **553**, 61 (2003) [arXiv:hep-ph/0210077].
- [11] C. P. Buszello, I. Fleck, P. Marquard and J. J. van der Bij, *Eur. Phys. J. C* **32**, 209 (2004) [arXiv:hep-ph/0212396].
- [12] W. Y. Keung, I. Low and J. Shu, *Phys. Rev. Lett.* **101**, 091802 (2008). [arXiv:0806.2864 [hep-ph]].
- [13] Q. H. Cao, C. B. Jackson, W. Y. Keung, I. Low and J. Shu, *Phys. Rev. D* **81**, 015010 (2010)

- [arXiv:0911.3398 [hep-ph]].
- [14] Y. Gao, A. V. Gritsan, Z. Guo, K. Melnikov, M. Schulze and N. V. Tran, Phys. Rev. D **81**, 075022 (2010) [arXiv:1001.3396 [hep-ph]].
- [15] A. De Rujula, J. Lykken, M. Pierini, C. Rogan and M. Spiropulu, Phys. Rev. D **82**, 013003 (2010) [arXiv:1001.5300 [hep-ph]].
- [16] J. F. Gunion and Z. Kunszt, Phys. Rev. D **33**, 665 (1986); M. J. Duncan, G. L. Kane and W. W. Repko, Nucl. Phys. B **272**, 517 (1986).
- [17] K. Hagiwara, R. D. Peccei, D. Zeppenfeld and K. Hikasa, Nucl. Phys. B **282**, 253 (1987).
- [18] K. Hagiwara and D. Zeppenfeld, Nucl. Phys. B **274**, 1 (1986).
- [19] See, for example, M. E. Peskin and D. V. Schroeder, “An Introduction to quantum field theory,” *Reading, USA: Addison-Wesley (1995) 842 p*
- [20] B. A. Kniehl, Nucl. Phys. B **352**, 1 (1991); D. Chang, W. Y. Keung and I. Phillips, Phys. Rev. D **48**, 3225 (1993). [arXiv:hep-ph/9303226]; V. D. Barger, K. M. Cheung, A. Djouadi, B. A. Kniehl and P. M. Zerwas, Phys. Rev. D **49**, 79 (1994); K. Hagiwara, S. Ishihara, J. Kamoshita and B. A. Kniehl, Eur. Phys. J. C **14**, 457 (2000) [arXiv:hep-ph/0002043]; V. Barger, T. Han, P. Langacker, B. McElrath and P. Zerwas, Phys. Rev. D **67**, 115001 (2003) [arXiv:hep-ph/0301097]; R. M. Godbole, D. J. . Miller and M. M. Muhlleitner, JHEP **0712**, 031 (2007) [arXiv:0708.0458 [hep-ph]]; S. Dutta, K. Hagiwara and Y. Matsumoto, Phys. Rev. D **78**, 115016 (2008) [arXiv:0808.0477 [hep-ph]].
- [21] V. Hankele, G. Klamke, D. Zeppenfeld and T. Figy, Phys. Rev. D **74**, 095001 (2006) [arXiv:hep-ph/0609075]; K. Hagiwara, Q. Li and K. Mawatari, JHEP **0907**, 101 (2009) [arXiv:0905.4314 [hep-ph]].
- [22] I. Low and J. Lykken, JHEP **1010**, 053 (2010) [arXiv:1005.0872 [hep-ph]].
- [23] K. Nakamura *et al.* [Particle Data Group], J. Phys. G **37**, 075021 (2010).
- [24] H. Muruyama. “Notes on Phase Space” Lecture notes. Accessible at <http://hitoshi.berkeley.edu/233B/phasespace.pdf>.
- [25] R. J. Barlow, Nucl. Instrum. Meth. A **297**, 496 (1990).
- [26] A. Djouadi, J. Kalinowski and M. Spira, Comput. Phys. Commun. **108**, 56 (1998) [arXiv:hep-ph/9704448].
- [27] R. Barate *et al.* [LEP Working Group for Higgs boson searches and ALEPH Collaboration and and], Phys. Lett. B **565**, 61 (2003) [arXiv:hep-ex/0306033].

- [28] V. Bartsch, G. Quast, “Expected signal observability at future experiments”, CMS-NOTE-2005-004 (2005).
- [29] H. L. Lai *et al.* [CTEQ Collaboration], *Eur. Phys. J. C* **12**, 375 (2000) [arXiv:hep-ph/9903282].
- [30] J. Alwall *et al.*, *JHEP* **0709**, 028 (2007) [arXiv:0706.2334 [hep-ph]].
- [31] G. L. Bayatian *et al.* [CMS Collaboration], CMS-TDR-008-1, 2006.
- [32] S. Catani, D. de Florian and M. Grazzini, *JHEP* **0201**, 015 (2002) [arXiv:hep-ph/0111164]; C. Anastasiou, K. Melnikov and F. Petriello, *Phys. Rev. Lett.* **93**, 262002 (2004) [arXiv:hep-ph/0409088]; G. Davatz, F. Stockli, C. Anastasiou, G. Dissertori, M. Dittmar, K. Melnikov and F. Petriello, *JHEP* **0607**, 037 (2006) [arXiv:hep-ph/0604077]; C. Anastasiou, G. Dissertori and F. Stockli, *JHEP* **0709**, 018 (2007) [arXiv:0707.2373 [hep-ph]]; C. Anastasiou, G. Dissertori, F. Stockli and B. R. Webber, *JHEP* **0803**, 017 (2008) [arXiv:0801.2682 [hep-ph]]; M. Grazzini, *JHEP* **0802**, 043 (2008) [arXiv:0801.3232 [hep-ph]]; C. Anastasiou, G. Dissertori, M. Grazzini, F. Stockli and B. R. Webber, *JHEP* **0908**, 099 (2009) [arXiv:0905.3529 [hep-ph]]; E. L. Berger, Q. H. Cao, C. B. Jackson, T. Liu and G. Shaughnessy, *Phys. Rev. D* **82**, 053003 (2010) [arXiv:1003.3875 [hep-ph]]; C. F. Berger, C. Marcantonini, I. W. Stewart, F. J. Tackmann and W. J. Waalewijn, *JHEP* **1104**, 092 (2011) [arXiv:1012.4480 [hep-ph]]; I. W. Stewart and F. J. Tackmann, arXiv:1107.2117 [hep-ph].
- [33] V. D. Barger, J. L. Lopez and W. Putikka, *Int. J. Mod. Phys. A* **3**, 2181 (1988).